BBA - Molecular Basis of Disease 1865 (2019) 2774–2787

Contents lists available at ScienceDirect

BBA - Molecular Basis of Disease

journal homepage: www.elsevier.com/locate/bbadis

Liver disease predominates in a mouse model for mild human Zellweger spectrum disorder☆

Kevin Berendse[a,b], Maxim Boek[a], Marion Gijbels[c], Nicole N. Van der Wel[d], Femke C. Klouwer[a,b], Marius A. van den Bergh-Weerman[d], Abhijit Babaji Shinde[e], Rob Ofman[a], Bwee Tien Poll-The[b], Sander M. Houten[f], Myriam Baes[e], Ronald J.A. Wanders[a], Hans R. Waterham[a,*]

[a] Amsterdam UMC, University of Amsterdam, Laboratory Genetic Metabolic Diseases, Amsterdam Gastroenterology & Metabolism, the Netherlands
[b] Emma Children's Hospital, Amsterdam UMC, University of Amsterdam, Paediatric Neurology, the Netherlands
[c] Department of Molecular Genetics, Cardiovascular Research Institute Maastricht, University of Maastricht, the Netherlands
[d] Amsterdam UMC, University of Amsterdam, Pathology, the Netherlands
[e] Department of Pharmaceutical and Pharmacological Sciences, Laboratory of Cell Metabolism, University of Leuven, Belgium
[f] Department of Genetics and Genomic Sciences, Icahn Institute for Genomics and Multiscale Biology, Icahn School of Medicine at Mount Sinai, New York, USA

ARTICLE INFO

Keywords:
Peroxisome biogenesis disorder
Peroxisome
Metabolism
Zellweger syndrome
Bile acid synthesis
Cholestasis

ABSTRACT

Zellweger spectrum disorders (ZSDs) are autosomal recessive diseases caused by defective peroxisome assembly. They constitute a clinical continuum from severe early lethal to relatively milder presentations in adulthood. Liver disease is a prevalent symptom in ZSD patients. The underlying pathogenesis for the liver disease, however, is not fully understood. We report a hypomorphic ZSD mouse model, which is homozygous for *Pex1*-c.2531G > A (p.G844D), the equivalent of the most common pathogenic variant found in ZSD, and which predominantly presents with liver disease. After introducing the Pex1-G844D allele by knock-in, we characterized homozygous Pex1-G844D mice for survival, biochemical parameters, including peroxisomal and mitochondrial functions, organ histology, and developmental parameters. The first 20 post-natal days (P20) were critical for survival of homozygous Pex1-G844D mice (~20% survival rate). Lethality was likely due to a combination of cholestatic liver problems, liver dysfunction and caloric deficit, probably as a consequence of defective bile acid biosynthesis. Survival beyond P20 was nearly 100%, but surviving mice showed a marked delay in growth. Surviving mice showed similar hepatic problems as described for mild ZSD patients, including hepatomegaly, bile duct proliferation, liver fibrosis and mitochondrial alterations. Biochemical analyses of various tissues showed the absence of functional peroxisomes accompanied with aberrant levels of peroxisomal metabolites predominantly in the liver, while other tissues were relatively spared.

ur findings show that homozygous Pex1-G844D mice have a predominant liver disease phenotype, mimicking the hepatic pathology of ZSD patients, and thus constitute a good model to study pathogenesis and treatment of liver disease in ZSD patients.

1. Introduction

Peroxisomes are organelles present in all cells, but most abundant in liver and kidney cells. They play an essential role in mammalian metabolism, including the α- and β-oxidation of very long chain, branched-chain and dicarboxylic fatty acids, and the synthesis of plasmalogens and bile acids [1]. The complete absence of functional peroxisomes results in multi-systemic disease and death in the first year of life, as is the case in the severe cerebro-hepato-renal or Zellweger syndrome (ZS; OMIM #601539). ZS represents the most severe presentation of the Zellweger spectrum disorders (ZSDs), which constitute a continuous biochemical and clinical spectrum of disease severity [2,3] and encompass, in decreasing severity, also the previously described clinical entities neonatal adrenoleukodystrophy (OMIM #214100), infantile Refsum disease (OMIM #266510), patients initially diagnosed with Usher syndrome [4] and Heimler syndrome (OMIM #616617 and

☆ Conflicts of interest: none.
Financial disclosure: none.

* Corresponding author at: Amsterdam UMC – University of Amsterdam, Laboratory Genetic Metabolic Diseases (F0-222), Amsterdam Gastroenterology & Metabolism, Meibergdreef 9, 1105 AZ Amsterdam, the Netherlands.
E-mail address: h.r.waterham@amc.uva.nl (H.R. Waterham).

https://doi.org/10.1016/j.bbadis.2019.06.013
Received 25 July 2018; Received in revised form 28 May 2019; Accepted 12 June 2019
Available online 15 June 2019

234580) [5].

ZSDs are caused by bi-allelic mutations in any of 13 different *PEX* genes, which encode proteins (peroxins) that cooperatively function in the assembly of peroxisomes, including the import of proteins and enzymes [6,7]. The defect in peroxisome assembly abrogates the metabolic functions of peroxisomes thus causing characteristic biochemical abnormalities. Accordingly, ZSDs are characterized by aberrant metabolite levels reflecting the peroxisomal dysfunction, including elevated plasma levels of very long-chain fatty acids (VLCFAs), the C_{27} bile acid precursors di- and trihydroxycholestanoic acid (DCHA and THCA), and pristanic- and phytanic acid, and decreased levels of C24 bile acids and docosahexaenoic acid (DHA), and plasmalogens in erythrocytes [1,2,7,8].

In addition to the often progressive neurological dysfunction impacting brain development, vision and hearing in ZSD patients, liver disease is a prevalent symptom [2,3,9–11]. The exact pathophysiological mechanism underlying the liver disease is unknown, but involves cholestasis that may be related to defective bile acid synthesis [12,13]. Bile acid synthesis is largely a hepatic process and requires functional peroxisomes [12]. In vitro studies previously showed that the C_{27} bile acid intermediates DHCA and THCA, which accumulate in ZSDs, are considerably more toxic than the normal C_{24} end products of bile acid synthesis cholic acid and chenodeoxycholic acid (14), but whether this causes the cholestasis has remained unresolved.

We generated a mouse model that is homozygous for the *Pex1*-c.2531G > A (p.G844D) allele (hereafter called Pex1-G844D mouse), which is the equivalent of the most common mutant allele found in human ZSD patients, i.e. PEX1-p.G843D. Approximately 60% of ZSD patients have bi-allelic mutations in the *PEX1* gene of whom 40% are compound heterozygous or homozygous for this allele [6,7,15]. PEX1 forms a heterohexamer with PEX6 to constitute the peroxisomal AAA ATPase complex, which is involved in the export of PEX5, the cytosolic receptor for PTS1-targeted peroxisomal matrix proteins, from the peroxisome back into the cytosol after delivery of its cargo [6,16]. A severe PEX1 defect completely impairs the import of peroxisomal matrix proteins resulting in the absence of protein-import competent peroxisomes. The PEX1-p.G843D mutation, however, affects the conformation and/or folding of the encoded PEX1 protein but still allows peroxisomal protein import, albeit impaired. The mutation typically results in peroxisome mosaicism in cell populations, with some cells having normal appearing peroxisomes while other cells have peroxisomal ghosts [6,17–19]. Patients homozygous for this mutation have a relatively mild phenotype and can survive into adulthood, while compound heterozygosity for this mutation results in an intermediate phenotype [20].

We here report the histological and biochemical characterization of a Pex1-G844D mouse model. Surprisingly, we found that in most organs and in cultured mouse embryonic fibroblasts (MEFs), peroxisomal functions were only mildly or even not affected. However, peroxisomal functions were markedly compromised in the liver resulting in cholestasis and the development of severe liver fibrosis, mimicking the liver pathology in ZSD patients. The Pex1-G844D mouse thus can be used to study the pathogenesis and treatment of liver disease in ZSDs.

2. Materials and methods

2.1. Generation and breeding of the Pex1-G844D mice

PEX1-G844D knock-in mice were generated for us by Taconic Artemis (Germany) on a pure C57BL/6N background. In brief, a targeting vector was generated using BAC clones from the C57BL/6 RPCIB-731 BAC library with the c.2531G > A variant coding for the p.G844D amino acid substitution introduced in exon 15 and the Puromycin resistance PuroR gene flanked by FRT sites inserted into intron 15 of *Pex1*. After confirmation by Sanger sequencing, the targeting vector was transfected into the Taconic Artemis C57BL/6N Tac ES cell line and homologous recombinant clones were isolated using positive (Puro R) and negative (Thymidine kinase) selection. Genotyping for the Pex1-c.2531G > A mutation in genomic DNA was performed by PCR using primers: 4737_35: ACAGGTAGCATGAACTAGATCGAG (P35) and 4737_36: CATTTGAGGTCATGATATTGCTG (P36) to yield products of 283 bp for the wild type and 358 bp for the Pex1- c.2531G > A knock-in (Fig. 1A). The presence of the c.2531G > A mutation in the Pex1 gene was verified by Sanger sequencing of the PCR products. Two confirmed ES clones were injected into C57BL/6N blastocysts for implantation. Resulting chimaeras were crossed with FLP-deleter mice to remove the selection markers followed by confirmation of germline transmission. After confirmation of Flp recombination of Puro R and thymidine kinase, the FlpE transgene was outcrossed in the PEX1-G844D line. Homozygous PEX1-G844D mice were obtained by intercrossing heterozygous PEX1-G844D mice; wild type littermates were used as controls. Routine genotyping of pups was performed by PCR analysis of genomic DNA using the above mentioned primers (Fig. 1A).

Mice were maintained in the animal housing facility of the Amsterdam UMC, University of Amsterdam at 21 °C ± 1 °C, 40–50% humidity, on a 12-h light-dark cycle, with ad libitum access to water and a standard rodent diet. All mouse studies were approved by the institutional review board for animal experiments of the Amsterdam UMC, University of Amsterdam and were carried out according to national ethical guidelines. To promote survival of the weaker Pex1-G844D pups, wild type and heterozygous littermates were removed from P3 to reach litters with a maximum of four pups. In addition, cages were equipped with electrical heating pads, Hydrogel and soft chow until weaning. Finally, weaning of Pex1-G844D pups was postponed until approximately P40. Experiments were performed with female mice, unless stated otherwise. Mice used for histological and/or biochemical analyses were first sedated using a 1:1 mixture of CO_2 and O_2, and then euthanized by 100% CO_2.

2.2. Generation and characterization of mouse embryonic fibroblasts

Mouse embryonic fibroblasts (MEFs) were isolated from E13 and E14 embryos [21] and immortalized to obtain stable cell lines [22] as described previously. MEFs were cultured at 37 °C in a humidified atmospheric environment with 5% CO_2, in Dulbecco's Modified Eagle's Medium (DMEM) supplemented with 10% fetal bovine serum, 25 mM HEPES buffer, 100 U/ml penicillin, 100 μg/ml streptomycin and amphotericin 250 μg/ml. For analysis, MEFs were harvested using trypsin (0.5% trypsin-EDTA, Invitrogen), washed once with phosphate-buffered saline (PBS) (Fresenius Kabi Nederland B·V.) and twice with 9 g/L NaCl (Fresenius Kabi Nederland B.V). MEFs were used for catalase immunofluorescence microscopy [5], immunoblot analysis [23], determination of VLCFA profiles [24], dihydroxyacetonephosphate-acyltransferase (DHAPAT) activity measurements [25], peroxisomal β-oxidation activity measurements using hexacosanoic acid (C26:0) and pristanic acid as substrates and mitochondrial β-oxidation activity measurements using hexadecanoic acid (C16:0) as substrate [24].

2.3. Histochemical analyses

For histochemical analyses we used at least three mice for each experimental group. Skin, skeleton, brain, heart, lung, spleen, stomach, intestine, liver, kidney, pancreas and testis of sacrificed mice were fixed in 4% paraformaldehyde for 7 days. After fixation, the organ samples were dehydrated through a graded series of ethanol and embedded in paraffin. Skeletal tissues were first decalcified in a solution of 40 g NaOH in 173 ml formic acid and 827 ml distilled water for 7 days prior to graded series of ethanol. Oil Red O staining was performed on frozen liver sections, and histological stainings, including hematoxylin and eosin (H&E), Fouchet, Sirius Red and Periodic acid–Schiff, on paraffin sections by the Pathology Department of the Amsterdam UMC, University of Amsterdam, The Netherlands, according to in-house protocols. All images were captured with a Leica microscope and

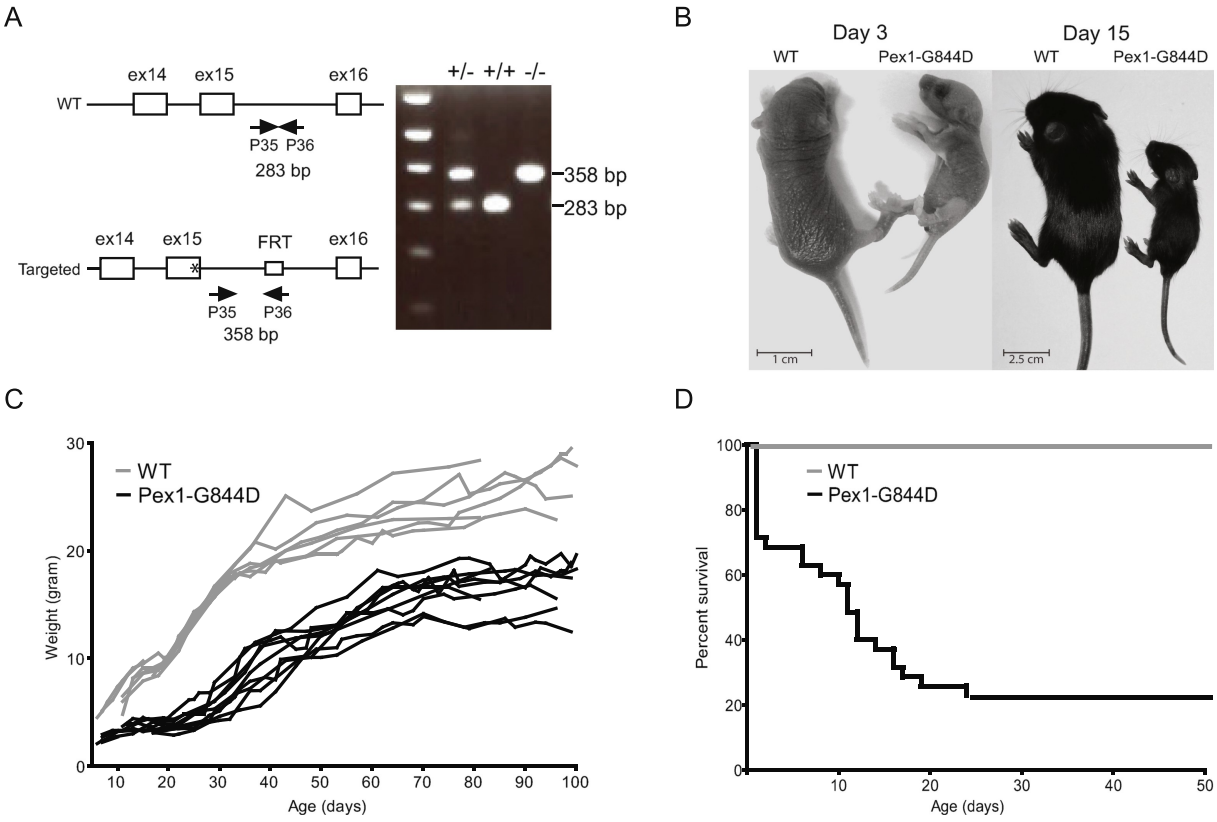

Fig. 1. Genotypic and phenotypic characterization of Pex1-G844D mice. (A) Schematic representation of the targeting of exon 15 of *Pex1* with wild type locus (top) and targeting allele (below). PCR amplification using primers P35 and P36 results in a 283 bp product from the wild type allele and a 358 bp product from the targeted allele (=Pex1-G844D). *, c. 2531A; FRT, flippase recognition target site; +, WT allele; −, Pex1-G844D allele. (B) Pex1-G844D mice displayed growth retardation starting at 3 days postnatal. (C) Individual growth curves of wild type and Pex1-G844D mice from 3 days to 100 days postnatal (both females and males combined). (D) Kaplan-Meier survival curve of both wild type (grey line) and Pex1-G844D mice (black line).

camera using Leica 4.1 software (Rijswijk, The Netherlands).

2.4. Immuno-EM and immunofluorescence analyses

Mouse liver samples were collected, fixed in duplicate in 0.2 M Pipes-Hepes-EGTA-MgCl2 (PHEM) buffer containing 4% paraformaldehyde either with or without 0.4% glutaraldehyde for 24 and 48 h, respectively. Subsequently, the liver samples were embedded in gelatin, cryosectioned with a Leica FCS and trimmed using a diamond Cryotrim 90 knife (Diatome, Switzerland) at −100 °C, and a Cryoimmuno knife (Diatome, Switzerland) at −120 °C to generate ultrathin sections of 50 nm, as described previously [26]. Immunogold labeling of the cryosections was performed using antiserum against ACAA1 (1:100 peroxisomal thiolase, Sigma-Aldrich, St Louis, Missouri, USA) and visualized with rabbit anti-mouse bridging serum (DAKO) and protein-A conjugated to 15 nm gold. All slides were examined with a FEI Tecnai 12 transmission electron microscope.

Immunofluorescence microscopy using monoclonal antibodies against peroxisomal catalase (mab 17E10, own production) and polyclonal antibodies against the peroxisomal membrane protein PMP70 (C-terminal epitope, obtained from Prof. Imanaka, Toyama, Japan) was performed as previously described [23] using a Leica TCS SP8 X Confocal Microscope.

2.5. Biochemical analyses

Levels of VLCFAs, phytanic and pristanic acid [27], bile acids [28], poly-unsaturated fatty acids and plasmalogens (C16:0- and C18:0-dimethyl acetal) [29] were determined in organs and/or plasma as previously described. C26:0-lysophosphatidylcholine was measured in bloodspots collected from 0 and 5 days old mice on filter paper (Whatman 903, GE LifeScience) [30]. Glucose was measured via a tail cut directly after sacrificing the mice. Activities of mitochondrial complex I-IV, citrate synthase and glutamate dehydrogenase (GDH) were measured in liver homogenates (40 to 80 mg) of 6 months old mice as described previously [31,32]. Immunoblot analysis using antibodies against PEX1 (1:250, BD Transduction laboratories, Franklin Lakes, New Jersey, USA) and peroxisomal thiolase (1:2000, *ACAA1*, Sigma-Aldrich, St Louis, Missouri, USA) was performed as described elsewhere [23]. Antigen-antibody complexes were visualized with IRDye 800CW 1:10,000 goat anti-rabbit and goat anti-mouse secondary antibodies, using the Odyssey Infrared Imaging System (LI-COR Biosciences, Nebraska, USA). Monoclonal anti-beta-actin antibody (1:20,000; Sigma-Aldrich, St Louis, Missouri, USA) was used as a loading control and visualized with IRDye 680RD donkey anti-mouse secondary antibody.

Protein band intensities were quantified with the Odyssey Infrared Imaging System software (LI-COR Biosciences, Lincoln, USA) and expressed as Integrated Intensity. Thiolase processing is expressed as the percentage Integrated Intensity of processed (41 kDa) over total (41kD + 44 kDa) thiolase protein.

2.6. Quantitative real-time RT-PCR

qRT-PCR was performed using an ABI PRISM 7500 Real Time PCR instrument (Applied Biosystems, Lennik, Belgium) as described previously [33]. The relative expression levels of the target genes were calculated as a ratio to the housekeeping gene β-actin.

2.7. Statistical analysis

For statistical analysis, two-tailed Student's *t*-tests or Chi square analysis were performed using Graphpad, software version 5.04, for Windows (GraphPad Software, La Jolla, California, USA). $P < 0.05$ was considered significant and for all experiments $n = 3$ was used, unless stated otherwise.

3. Results

3.1. Generation and phenotype of Pex1-G844D mice

To generate a mouse model for the most common genotype associated with a relatively mild presentation of ZSD, i.e. homozygosity for *PEX1*-c.2528G > A (p.G843D) [6,7,15], we introduced, by knock-in, the c.2531G > A (p.G844D) mutation in exon 15 of the *Pex1* gene in mice on a pure C57BL/6N background. Genotyping of the offspring of intercrossed heterozygous Pex1-G844D mice at postnatal day 0–5 yielded 127 wild type, 278 heterozygous, and 82 (homozygous) Pex1-G844D mice ($n = 487$), resulting in a genotypic ratio of 1:2.2:0.65, indicating significant embryonic and/or perinatal loss of homozygous mutant mice (Chi square = 18, $P < 0.005$). At P0, no marked difference in size and weight was observed between wild type, heterozygous and Pex1-G844D littermates. At P3, however, the Pex1-G844D pups were clearly smaller, weighed less (Fig. 1B) and appeared very weak when compared to their wild type and heterozygous littermates, despite the observation of “normal”-looking milk spots in their stomachs. In the first 100 postnatal days, both female and male Pex1-G844D mice showed a marked growth delay when compared to wild type mice (ig. 1C). The first 20 postnatal days were found most critical; ~75% of the Pex1-G844D mice died before P20 (Fig. 1D). After these first 20 days, survival was 90% ($n = 10$; one Pex1-G844D mice died at 187exdays of age). The growth delay of the Pex1-G844D mice remained evident throughout life, but the mutant mice showed a similar growth pattern as wild type animals with a clear growth spurt between 20 and 50days (Fig. 1C).

Albeit delayed, we observed that Pex1-G844D males were fertile ($n = 4$) and able to produce offspring after approximately 5 months of age. Because of their small size we did not examine whether Pex1-G884D female mice were also able to produce offspring.

3.2. Analysis of mouse embryonic fibroblasts (MEFs)

The PEX1-p.G843D mutation in human cells is associated with peroxisomal mosaicism, a phenomenon in which a subset of the cells still contains functional peroxisomes whereas others do not [30]. Cells without functional peroxisomes still have peroxisomal vesicles containing peroxisomal membrane proteins but lack matrix proteins. To determine whether peroxisomal mosaicism also occurs in the Pex1-G844D MEFs, we performed immunofluorescence microscopy using antibodies against the peroxisomal matrix protein catalase and the peroxisomal membrane protein PMP70. The majority of cells contained both catalase- and PMP70-positive peroxisomes, while a minor portion (5–10%) showed catalase-deficient but PMP70-positive peroxisomal vesicles, indicating a low degree of peroxisomal mosaicism (for example see Fig. 2A). When the MEFs were cultured at 40 °C, however, a marked increase in cells with catalase-deficient peroxisomal vesicles was observed, analogous to human patient skin fibroblasts homozygous for PEX1-p.G843D [17–19 and data not shown).

Because the peroxisomal matrix enzyme thiolase is processed from a 44-kDa precursor form to a 41-kDa mature form only after its import into peroxisomes [34], thiolase processing can be used as a sensitive marker for functional protein import-competent peroxisomes [19]. Thiolase processing was examined by immunoblot analysis of MEFs cultured at 37 °C and 40 °C (Fig. 2B). The amount of processed thiolase (41-kDa) was lower and a weak 44-kDa band could be observed at 37 °C in the Pex1-G844D MEFs when compared to wild type MEFs. Culturing of the MEFs at 40 °C resulted in a markedly impaired thiolase processing in the Pex1-G844D but not in wild type MEFs, confirming the temperature sensitivity of the Pex1-G844D mutation.

When we analyzed different peroxisomal functions and parameters in the MEFs (Table 1), we observed a significant decrease in the activity of dihydroxyacetonephosphate-acyltransferase (DHAPAT), a peroxisomal enzyme involved in plasmalogen synthesis, in Pex1-G844D compared to wild type MEFs. Whereas the peroxisomal β-oxidation rate of pristanic acid was significantly decreased in the Pex1-G844D MEFs, the degradation of C26:0 was not impaired. This corresponds with an unaltered C26:0 over C22:0 (docosanoic acid) ratio between wild type and Pex1-G844D MEFs when cultured at 37 °C. However, this ratio significantly increased in Pex1-G844D MEFs after culturing the cells at 40 °C (Table 1). The degradation of palmitate (C16:0) via mitochondrial β-oxidation was not impaired in the Pex1-G844D MEFs.

3.3. Biochemical analysis of Pex1-G844D mice tissues

We first studied the consequences of the Pex1-G844D protein on peroxisomal matrix protein import in different tissues using thiolase processing as read out. Analyses of thiolase processing in tissues from 10 days old mice showed a complete defect in processing in liver samples and a partial defect in heart samples of the Pex1-G844D mice (Fig. 2D), whereas thiolase processing was unchanged and complete in brain, spleen and kidney samples of both the Pex1-G844D and wild type mice. Of note, we observed that total thiolase protein levels were lowered in brain, spleen and heart tissue, but unchanged or somewhat increased in liver and kidney of the Pex1-G844D mice. The defect in thiolase processing in the liver samples occurred despite the presence of mutant Pex1 protein levels that were comparable to the levels in control mice, which also had been observed previously in human cells homozygous for the PEX1-p.G843D mutation [19] (Supplemental Fig. 1A). Thiolase processing was also completely defective in liver samples of 6 months old Pex1-G844D mice while the total thiolase protein levels were lowered in the Pex1-G844D mice. In brain and heart samples the thiolase processing was similar as in wild type mice of this age (Fig. 2C).

Because we observed a critical survival phase of the mice between 0 and 20 days, we performed detailed biochemical analyses of liver, brain, spleen, heart and kidney tissue (Table 2) of Pex1-G844D and wild type mice aged 0, 5, 10 and 15 days, and 3 and 6 months. Overall, we found the most striking peroxisomal metabolite abnormalities in the livers of Pex1-G844D mice at all ages, which is in line with the complete defect of thiolase processing observed in this tissue.

Analyses of very long chain fatty acids (Table 2A), which are specific substrates for peroxisomal β-oxidation, revealed significantly elevated levels of C26:0 and increased C26:0/C22:0 ratios in liver samples of the Pex1-G844D mice at all, respectively most ages. For most other tissues these levels were not significantly different between Pex1-G844D and wild type mice. Analysis of blood spots from the Pex1-G844D mice showed highly significantly elevated levels of C26:0-lysophosphatidylcholine (C26:0-lysoPC) in keeping with the notion that C26:0-lysoPC is currently considered the most sensitive diagnostic marker for a ZSD [35].

The levels of the branched-chain fatty acids phytanic and pristanic acid (Table 2A), substrates for peroxisomal α- and β-oxidation respectively and present in low levels in normal chow, were both increased in the livers of 3- and 6-months old Pex1-G844D mice. In livers of 3- and 6-months old wild type mice, pristanic acid was undetectable. Phytanic acid was also undetectable in livers of 3-months old wild type mice, but low levels were detected in livers of 6-months old wild type mice.

The levels of the poly-unsaturated fatty acid docosahexaenoic acid (DHA; Table 2B), the synthesis of which requires a single peroxisomal β-oxidation cycle, were reduced in most tissues of the Pex1-G844D mice at all ages, although it did not always reach statistical significance.

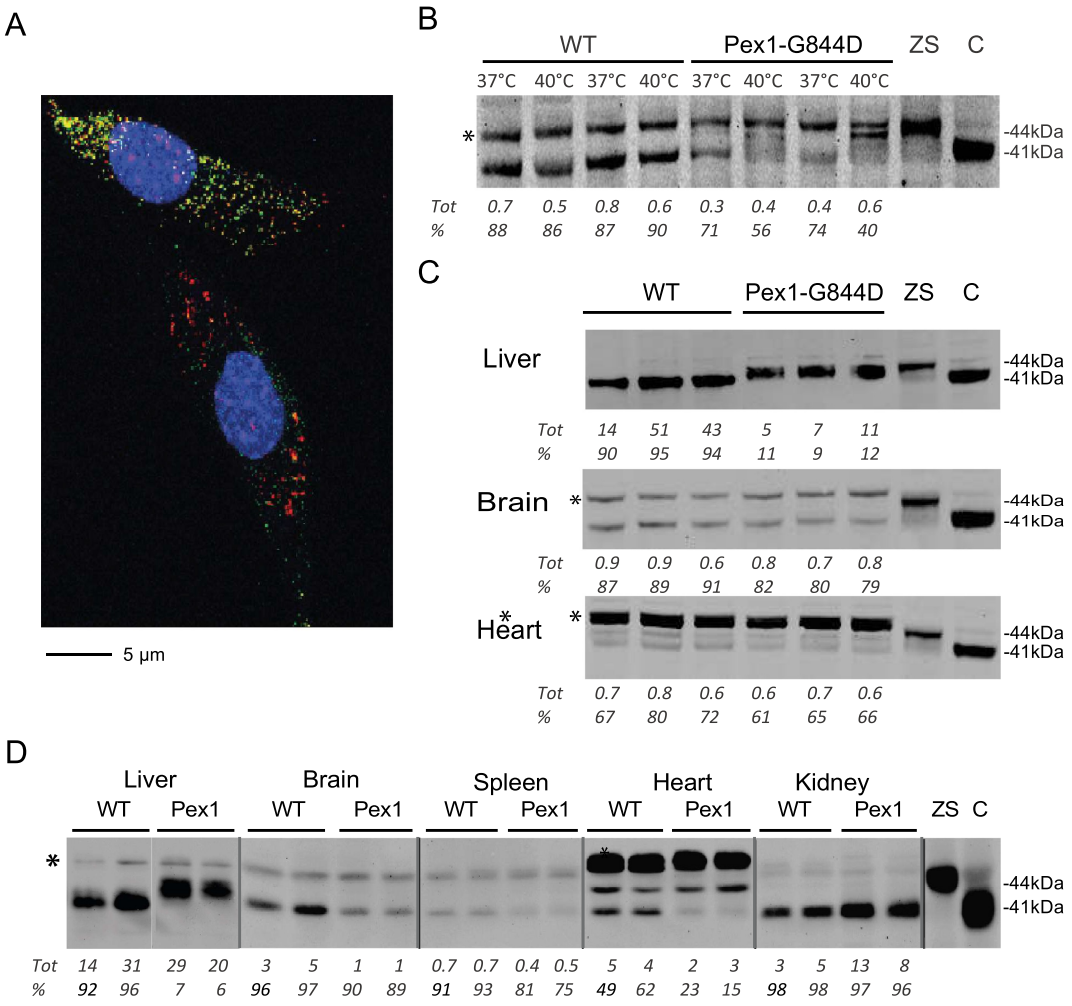

Fig. 2. Characterization of MEFs and tissues from wild type and Pex1-G844D mice. (A) Merged immunofluorescence microscopy image of Pex1-G844D MEFs cultured at 37 °C showing peroxisomal mosaicism after staining with antibodies against the peroxisomal matrix protein catalase (green) and the peroxisomal membrane protein PMP70 (red). (B) Western blot analysis of homogenates (50 μg of protein) of Pex1-G844D (n = 2) and wild type (n = 2) MEFs cultured at 37 °C and 40 °C and human skin fibroblasts cultured at 37 °C using a peroxisomal thiolase antibody showed increased defective thiolase processing in Pex1-G844D MEFs at 40 °C. Protein band intensities were quantified with the Odyssey Infrared Imaging System software (LI-COR Biosciences, Lincoln, USA) and expressed as Integrated Intensity. Thiolase processing is expressed as the percentage Integrated Intensity of processed (41 kDa) over total (41kD + 44 kDa) thiolase protein. ZS, fibroblasts from severe Zellweger syndrome patient; C, human control fibroblasts; *, denotes a cross-reacting protein of unknown identity (~46 kDa); 44 kDa, unprocessed thiolase; 41 kDa, processed thiolase; Tot, total thiolase protein (41 kDa + 44 kDa); %, percentage processed (41 kDa) of total thiolase protein (41 kDa + 44 kDa). (C) Western blot analysis of liver (5 μg of protein), brain (40 μg of protein) and heart (40 μg of protein) homogenates of 6- months old Pex1-G844D and wild type (WT) mice using a peroxisomal thiolase antibody showed defective thiolase processing in Pex1-G844D liver, but no difference in processing in the other tissues. Labelling as under (B). (D) Western blot analysis of liver (10 μg of protein), brain (40 μg of protein), spleen (40 μg of protein), heart (40 μg of protein) and kidney (15 μg of protein) homogenates of 10-days old Pex1-G844D and wild type (WT) mice using a peroxisomal thiolase antibody shows defective thiolase processing in Pex1-G844D liver and a partial defect in Pex1-G844D heart, but no difference in processing in the other tissues. Labelling as under (B).

Table 1
Biochemical analysis in MEFs from wild type and homozygous Pex1-G844D mice.

	WT	Pex1-G844D	*P value*
DHAPAT activity (pmol/h·mg)	**13.2 ± 2.7**	**4.9 ± 1.8**	***0.011***
C16:0 oxidation (nmol/h·mg)	15.77 ± 4.21	18.80 ± 2.26	*0.334*
C26:0 oxidation (nmol/h·mg)	1.05 ± 0.18	0.91 ± 0.10	*0.286*
Pristanic acid oxidation (nmol/h·mg)	**0.98 ± 0.38**	**0.23 ± 0.03**	***0.027***
C26:0/C22:0, 40°C versus 37°C (fold increase)	**0.40 ± 0.07**	**1.95 ± 0.43**	***0.004***

Shown are mean + SD (n = 3). Significant changes with P values < 0.05 are displayed in bold.

The conversion of C_{27}-bile acid precursors into mature C_{24}-bile acids is dependent on peroxisomal β-oxidation and occurs exclusively in liver. Bile acid analysis revealed significant elevations of unconjugated and tauro-conjugated C_{27}-bile acids and concomitantly decreased levels of tauro-conjugated C_{24}-bile acids in the liver samples of the Pex1-G844D mice at all ages (Table 2C). Furthermore, we found significantly increased levels of unconjugated C_{27}-bile acids and significantly decreased levels of tauro-conjugated C_{24}-bile acids in plasma of Pex1-G844D mice at P10 but not in plasma of adult mice. Similar as observed in patients with a ZSD [13,14], we noted that the C_{27}-bile acids in the Pex1-G844D liver samples primarily occurred in the unconjugated form, most probably due to a deficiency of the liver-specific peroxisomal enzyme bile acid-coenzyme A: amino acid N-acyl transferase (BAAT), which catalyzes this conjugation. In keeping with this, the C_{24}-

Table 2
Biochemical analysis in liver, brain, spleen, heart and kidney homogenates, and plasma and bloodspots of wild type and homozygous Pex1-G844D mice.

A. Very long-chain and branched-chain fatty acids

C26:0

	Day 0			Day 5			Day 10		
	Pex1-G844D	WT	*P value*	Pex1-G844D	WT	*P value*	Pex1-G844D	WT	*P value*
Liver	**0.31 ± 0.06**	**0.06 ± 0.04**	***2 × 10–4***	**0.12 ± 0.05**	**0.03 ± 0.01**	***0.04***	**0.06 ± 0**	**0.03 ± 0**	***1 × 10–4***
Brain	0.02 ± 0.01	0.02 ± 0.00	*0.095*	0.02 ± 0.00	0.02 ± 0.00	*0.519*	**0.04 ± 0.01**	**0.02 ± 0.00**	***0.003***
Spleen	n/a	n/a		0.03 ± 0.00	0.02 ± 0.00	*0.058*	0.04 ± 0.01	0.02 ± 0.00	*0.071*
Heart	0.04 ± 0.02	0.02 ± 0.00	*0.087*	0.02 ± 0.00	0.06 ± 0.06	*0.434*	0.01 ± 0.00	0.02 ± 0.00	*0.158*
Kidney	0.04 ± 0.04	0.04 ± 0.02	*1.000*	0.02 ± 0.00	0.02 ± 0.00	*0.219*	0.03 ± 0.02	0.02 ± 0.00	*0.270*

C26:0/C22:0

	Day 0			Day 5			Day 10		
	Pex1-G844D	WT	*P value*	Pex1-G844D	WT	*P value*	Pex1-G844D	WT	*P value*
Liver	**0.35 ± 0.03**	**0.09 ± 0.08**	***2.9 × 10–4***	0.30 ± 0.14	0.17 ± 0.04	*0.19*	0.09 ± 0.01	0.13 ± 0.03	*0.08*
Brain	**0.18 ± 0.04**	**0.11 ± 0.03**	***0.014***	0.15 ± 0.03	0.15 ± 0.05	*0.865*	0.15 ± 0.07	0.13 ± 0.00	*0.619*
Spleen	n/a	n/a		**0.19 ± 0.00**	**0.10 ± 0.01**	***0.001***	0.15 ± 0.04	0.08 ± 0.01	*0.066*
Heart	**0.15 ± 0.04**	**0.07 ± 0.01**	***0.013***	0.08 ± 0.01	0.22 ± 0.2	*0.484*	0.07 ± 0.01	0.06 ± 0.01	*0.078*
Kidney	0.08 ± 0.02	0.09 ± 0.07	*0.947*	**0.03 ± 0.00**	**0.02 ± 0.00**	***0.030***	0.04 ± 0.02	0.02 ± 0.01	*0.226*

C26:0-lysoPC

	Day 0			Day 5		
	Pex1-G844D	WT	*P value*	Pex1-G844D	WT	*P value*
Bloodspot	**1458 ± 340**	**87 ± 22**	***0.0001***	**489 ± 35**	**26 ± 8**	***8.8 × 10–8***

Phytanic acid

	Day 0			Day 5			Day 10		
	Pex1-G844D	WT	*P value*	Pex1-G844D	WT	*P value*	Pex1-G844D	WT	*P value*
Liver	n/a	n/a		n/a	n/a		n/a	n/a	

Pristanic acid

	Day 0			Day 5			Day 10		
	Pex1-G844D	WT	*P value*	Pex1-G844D	WT	*P value*	Pex1-G844D	WT	*P value*
Liver	n/a	n/a		n/a	n/a		n/a	n/a	

A. Very long-chain and branched-chain fatty acids

C26:0

	Day 15			3 months			6 months		
	Pex1-G844D	WT	*P value*	Pex1-G844D	WT	*P value*	Pex1-G844D	WT	*P value*
Liver	**0.07 ± 0.01**	**0.04 ± 0.01**	***0.01***	**0.09 ± 0.01**	**0.02 ± 0**	***1.1 × 10–3***	**0.09 ± 0.01**	**0.01 ± 0**	***3 × 10–5***
Brain	0.08 ± 0.06	0.05 ± 0.00	*0.530*	0.07 ± 0.06	0.03 ± 0.01	*0.293*	0.04 ± 0.04	0.04 ± 0.03	*0.887*
Spleen	**0.09 ± 0.04**	**0.02 ± 0.00**	***0.045***	n/a	n/a		**0.13 ± 0.02**	**0.05 ± 0.03**	***0.005***
Heart	0.01 ± 0.00	0.01 ± 0.00	*1.000*	0.03 ± 0.02	0.01 ± 0.00	*0.322*	0.02 ± 0.01	0.01 ± 0.00	*0.305*
Kidney	0.09 ± 0.08	0.04 ± 0.02	*0.288*	0.07 ± 0.04	0.03 ± 0.01	*0.176*	0.07 ± 0.05	0.05 ± 0.03	*0.653*

C26:0/C22:0

	Day 15			3 months			6 months		
	Pex1-G844D	WT	*P value*	Pex1-G844D	WT	*P value*	Pex1-G844D	WT	*P value*
Liver	0.11 ± 0.2	0.11 ± 0.0	*0.9*	**0.12 ± 0.0**	**0.05 ± 0.01**	***1.7 × 10–3***	**0.12 ± 0.02**	**0.04 ± 0.01**	***1.6 × 10–3***
Brain	0.32 ± 0.2	0.08 ± 0.05	*0.229*	0.04 ± 0.01	0.04 ± 0.01	*0.805*	0.03 ± 0.01	0.02 ± 0.01	*0.406*
Spleen	**0.26 ± 0.08**	**0.05 ± 0.01**	***0.012***	n/a	0.05 ± 0.00		**0.27 ± 0.07**	**0.07 ± 0.03**	***0.005***
Heart	0.07 ± 0.01	0.08 ± 0.05	*0.786*	**0.06 ± 0.01**	**0.03 ± 0.00**	***0.003***	0.04 ± 0.01	0.03 ± 0.00	*0.458*
Kidney	0.06 ± 0.03	0.01 ± 0.00	*0.070*	0.04 ± 0.02	0.02 ± 0.00	*0.207*	0.03 ± 0.02	0.02 ± 0.01	*0.492*

(*continued on next page*)

Table 2 (*continued*)

A. Very long-chain and branched-chain fatty acids

C26:0-lysoPC

Bloodspot

Phytanic acid

	Day 15			3 months			6 months		
	Pex1-G844D	WT	*P value*	Pex1-G844D	WT	*P value*	Pex1-G844D	WT	*P value*
Liver	n/a	n/a		**0.23 ± 0.03**	**0 ± 0**	***1.8 × 10–4***	**0.39 ± 0.05**	**0.02 ± 0**	***1.9 × 10–4***

Pristanic acid

	Day 15			3 months			6 months		
	Pex1-G844D	WT	*P value*	Pex1-G844D	WT	*P value*	Pex1-G844D	WT	*P value*
Liver	n/a	n/a		**0.13 ± 0.03**	**0 ± 0**	***0.027***	**0.22 ± 0.03**	**0 ± 0**	***1.4 × 10–4***

B. Poly unsaturated fatty acids

DHA

	Day 0			Day 5			Day 10		
	Pex1-G844D	WT	*P value*	Pex1-G844D	WT	*P value*	Pex1-G844D	WT	*P value*
Liver	**38.8 ± 5.0**	**20.6 ± 2.3**	***2.8 × 10–4***	**39.7 ± 3.8**	**75.7 ± 6.6**	***1.2 × 10–3***	28.5 ± 11.2	51.9 ± 31.3	*0.29*
Brain	24.3 ± 3.4	22.4 ± 9.3	*0.691*	40.3 ± 4.1	39.1 ± 2.7	*0.693*	**34.7 ± 6.9**	**48.3 ± 4.5**	***0.046***
Spleen	n/a	n/a		3.25 ± 0.6	11.1 ± 6.0	*0.179*	**3.6 ± 0.6**	**7 ± 1.1**	***0.032***
Heart	11.3 ± 0.6	9.6 ± 2.2	*0.183*	19.2 ± 3.1	23.5 ± 2.1	*0.151*	**9.2 ± 2.7**	**31.3 ± 2.9**	***0.001***
Kidney	12.2 ± 3.3	12.0 ± 1.8	*0.940*	15.7 ± 3.1	21.4 ± 5.3	*0.181*	**17.6 ± 1.2**	**23.1 ± 1.8**	***0.012***

B. Poly unsaturated fatty acids

DHA

	Day 15			3 months			6 months		
	Pex1-G844D	WT	*P value*	Pex1-G844D	WT	*P value*	Pex1-G844D	WT	*P value*
Liver	30.0 ± 3.2	49.0 ± 15.9	*0.11*	43.4 ± 13.7	29.7 ± 4.2	*0.17*	47.9 ± 12.1	43.1 ± 4.3	*0.55*
Brain	**28.9 ± 16.2**	**72.5 ± 10.7**	***0.004***	92.2 ± 37.6	116.3 ± 25.3	*0.410*	109.0 ± 10.8	119.3 ± 6.8	*0.210*
Spleen	**3.7 1.3)**	**11.5 ± 1.7**	***0.003***	9.1 (n = 1)	4.5 (n = 1)		**8.3 ± 4.4**	**14.2 ± 1.6**	***0.012***
Heart	12.9 ± 4.8	22.7 ± 13.0	*0.284*	57.7 ± 7.8	81.2 ± 20.6	*0.237*	**40.6 ± 4.3**	**61.9 ± 14.7**	***0.037***
Kidney	23.6 ± 7.6	49.3 ± 44.1	*0.376*	33.5 ± 12.9	44.2 ± 5.6	*0.258*	**31.0 ± 8.1**	**52.0 ± 10.8**	***0.031***

C. Bile acids

Unconjugated C24-bile acids

	Day 0			Day 5			Day 10		
	Pex1-G844D	WT	*P value*	Pex1-G844D	WT	*P value*	Pex1-G844D	WT	*P value*
Liver	**22.9 ± 7.7**	**12.3 ± 2.9**	***0.03***	**0.5 ± 0.8**	**57.2 ± 18.7**	***6.3 × 10–3***	**1.9 ± 1.7**	**78.5 ± 11.7**	***3.6 × 10–4***
Brain	0 ± 0	0 ± 0		0 ± 0	0 ± 0		0 ± 0	0 ± 0	
Spleen	n/a	n/a		n/a	n/a		n/a	n/a	
Heart	n/a	n/a		n/a	n/a		n/a	n/a	
Kidney	n/a	n/a		n/a	n/a		n/a	n/a	
Plasma	n/a	n/a		n/a	n/a		0.08 ± 0.03	0.06 ± 0.00	*0.3918*

Tauro-conjugated C24-bile acids

	Day 0			Day 5			Day 10		
	Pex1-G844D	WT	*P value*	Pex1-G844D	WT	*P value*	Pex1-G844D	WT	*P value*

(*continued on next page*)

Table 2 (*continued*)

C. Bile acids

Liver	**133 ± 39**	**1365 ± 588**	***2.1 × 10–3***	**265 ± 171**	**1758 ± 639**	***0.02***	**168 ± 66**	**1423 ± 407**	***6.2 × 10–3***
Brain	0 ± 0	0 ± 0	0 ± 0	0 ± 0	0 ± 0		0 ± 0	0 ± 0	
Spleen	n/a	n/a		n/a	n/a		n/a	n/a	
Heart	n/a	n/a		n/a	n/a		n/a	n/a	
Kidney	n/a	n/a		n/a	n/a		n/a	n/a	
Plasma	n/a	n/a		n/a	n/a		**0.95 ± 0.59**	**8.44 ± 1.57**	***0.013***
Unconjugated C27-bile acids									
	Day 0			Day 5			Day 10		
	Pex1-G844D	WT	*P value*	Pex1-G844D	WT	*P value*	Pex1-G844D	WT	*P value*
Liver	**294 ± 41**	**1.5 ± 1.0**	***2.3 × 10–6***	**238 ± 101**	**0.5 ± 0.9**	***1.5 × 10–2***	**290 ± 57**	**0 ± 0**	***9.0 × 10–4***
Brain	0 ± 0	0 ± 0		0 ± 0	0 ± 0		0 ± 0	0 ± 0	
Spleen	n/a	n/a		n/a	n/a		n/a	n/a	
Heart	n/a	n/a		n/a	n/a		n/a	n/a	
Kidney	n/a	n/a		n/a	n/a		n/a	n/a	
Plasma	n/a	n/a		n/a	n/a		**1.80 ± 0.56**	**0.34 ± 0.11**	***0.040***
Tauro-conjugated C27-bile acids									
	Day 0			Day 5			Day 10		
	Pex1-G844D	WT	*P value*	Pex1-G844D	WT	*P value*	Pex1-G844D	WT	*P value*
Liver	**2.9 ± 1.9**	**0 ± 0**	***0.02***	15.6 ± 14	0.5 ± 0.9	*0.13*	**28.8 ± 10.2**	**0 ± 0**	***8.2 × 10–3***
Brain	0 ± 0	0 ± 0		0 ± 0	0 ± 0		0 ± 0	0 ± 0	
Spleen	n/a	n/a		n/a	n/a		n/a	n/a	
Heart	n/a	n/a		n/a	n/a		n/a	n/a	
Kidney	n/a	n/a		n/a	n/a		n/a	n/a	
Plasma	n/a	n/a		n/a	n/a		0 ± 0	0 ± 0	

C. Bile acids

Unconjugated C24-bile acids									
	Day 15			3 months			6 months		
	Pex1-G844D	WT	*P value*	Pex1-G844D	WT	*P value*	Pex1-G844D	WT	*P value*
Liver	1.4 ± 1.5	21.3 ± 15.7	*0.09*	179 ± 250	169 ± 116	*0.95*	77.7 ± 60.9	13.4 ± 6	*0.14*
Brain	0 ± 0	0 ± 0		0 ± 0	0 ± 0		0 ± 0	0 ± 0	
Spleen	n/a	n/a		n/a	n/a		7.80 ± 5.09	2.17 ± 2.31	*0.139*
Heart	n/a	n/a		6.0 ± 6.8	77.0 ± 118	*0.357*	n/a	n/a	
Kidney	n/a	n/a		3.47 ± 4.23	15.05 ± 18.9	*0.360*	35.60 ± 30.29	2.43 ± 2.43	*0.124*
Plasma	n/a	n/a		1.79 ± 1.22	1.13 ± 0.93	*0.493*	4.55 ± 4.60	0.63 ± 0.32	*0.210*
Tauro-conjugated C24-bile acids									
	Day 15			3 months			6 months		
	Pex1-G844D	WT	*P value*	Pex1-G844D	WT	*P value*	Pex1-G844D	WT	*P value*
Liver	**151 ± 21**	**1283 ± 362**	***5.6 × 10–3***	58 ± 52	739 ± 716	*0.18*	221 ± 110	1391 ± 980	*0.06*
Brain	0 ± 0	0 ± 0		0 ± 0	0 ± 0		0 ± 0	0 ± 0	
Spleen	n/a	n/a		n/a	n/a		5.54 ± 8.71	47.83 ± 62.7	*0.227*
Heart	n/a	n/a		17.1 ± 6.9	14.6 ± 12.8	*0.783*	n/a	n/a	
Kidney	n/a	n/a		45.32 ± 22.7	22.5 ± 22.8	*0.287*	23.94 ± 12.58	73.25 ± 95.9	*0.341*
Plasma	n/a	n/a		6.93 ± 8.84	3.42 ± 3.11	*0.552*	4.43 ± 4.16	1.53 ± 1.69	*0.314*
Unconjugated C27-bile acids									
	Day 15			3 months			6 months		
	Pex1-G844D	WT	*P value*	Pex1-G844D	WT	*P value*	Pex1-G844D	WT	*P value*
Liver	**227 ± 83**	**0.9 ± 1.5**	***9.1 × 10–3***	**211 ± 13**	**0 ± 0**	***1.1 × 10–5***	**159 ± 35**	**0 ± 0**	***6.0 × 10–4***
Brain	0 ± 0	0 ± 0		0 ± 0	0 ± 0		0 ± 0	0 ± 0	
Spleen	n/a	n/a		n/a	n/a		**13.41 ± 7.95**	**0 ± 0**	***0.036***
Heart	n/a	n/a		**30.7 ± 11.5**	**0 ± 0**	***0.010***	n/a	n/a	

(*continued on next page*)

Table 2 (*continued*)

C. Bile acids									
Kidney	n/a	n/a		**57.1 ± 21.4**	**0 ± 0**	***0.010***	**52.71 ± 24.5**	**0 ± 0**	***0.015***
Plasma	n/a	n/a		**17.52 ± 5.13**	**0.23 ± 0.02**	***0.004***	**20.41 ± 7.69**	**0.44 ± 0.05**	***0.007***
Tauro-conjugated C27-bile acids									
	Day 15			3 months			6 months		
	Pex1-G844D	WT	*P value*	Pex1-G844D	WT	*P value*	Pex1-G844D	WT	*P value*
Liver	24.2 ± 16.1	0 ± 0	*0.06*	**5.4 ± 2.2**	**0.9 ± 1.5**	***0.04***	10.9 ± 13.6	0.1 ± 0.2	*0.24*
Brain	0 ± 0	0 ± 0		0 ± 0	0 ± 0		0 ± 0	0 ± 0	
Spleen	n/a	n/a		n/a	n/a		0 ± 0	0 ± 0	
Heart	n/a	n/a		0 ± 0	0 ± 0		n/a	n/a	
Kidney	n/a	n/a		0 ± 0	0 ± 0		0 ± 0	0 ± 0	
Plasma	n/a	n/a		0 ± 0	0 ± 0		0 ± 0	0 ± 0	

D. Plasmalogens									
C16 DMA/C16:0									
	Day 0			Day 5			Day 10		
	Pex1-G844D	WT	*P value*	Pex1-G844D	WT	*P value*	Pex1-G844D	WT	*P value*
Liver	**0.96 ± 0.09**	**2.10 ± 0.32**	***1.1 × 10–4***	0.60 ± 0.20	0.70 ± 0.30	*0.66*	0.67 ± 0.06	0.90 ± 0.17	*0.09*
Brain	5.9 ± 0.6	5.5 ± 0.2	*0.294*	**5.2 ± 0.3**	**5.8 ± 0.1**	***0.021***	6.0 ± 1.2	5.8 ± 0.4	*0.837*
Spleen	n/a	n/a		5.15 ± 1.3	4.8 ± 1.7	*0.719*	6.0 ± 1.1	7.6 ± 1.2	*0.239*
Heart	11.5 ± 0.5	11.6 ± 1.2	*0.970*	8.0 ± 1.0	5.2 ± 0.6	*0.645*	7.3 ± 0.9	8.4 ± 0.9	*0.192*
Kidney	5.8 ± 0.4	5.8 ± 0.5	*1.000*	6.2 ± 1.0	4.1 ± 1.1	*0.076*	4.7 ± 0.5	4.1 ± 2.1	*0.667*
C18 DMA/C18:0									
	Day 0			Day 5			Day 10		
	Pex1-G844D	WT	*P value*	Pex1-G844D	WT	*P value*	Pex1-G844D	WT	*P value*
Liver	**0.7 ± 0.07**	**1.33 ± 0.46**	***0.01***	0.50 ± 0.14	0.35 ± 0.07	*0.31*	0.40 ± 0.17	0.47 ± 0.06	*0.56*
Brain	6.0 ± 0.7	6.6 ± 0.4	*0.182*	7.2 ± 0.8	7.8 ± 1.2	*0.502*	8.5 ± 1.2	6.9 ± 0.9	*0.135*
Spleen	n/a	n/a		3.7 ± 0.9	3.7 ± 0.6	*0.425*	4.1 ± 1.3	5.2 ± 0.4	*0.365*
Heart	2.9 ± 0.2	3.2 ± 0.5	*0.310*	2.0 ± 0.5	1.8 ± 0.2	*0.220*	1.3 ± 0.2	1.3 ± 0.1	*0.768*
Kidney	6.0 ± 0.7	6.3 ± 0.5	*0.545*	6.6 ± 3.8	6.3 ± 0.5	*0.464*	**5.9 ± 0.2**	**7.0 ± 0.6**	***0.048***

D. Plasmalogens									
C16 DMA/C16:0									
	Day 15			3 months			6 months		
	Pex1-G844D	WT	*P value*	Pex1-G844D	WT	*P value*	Pex1-G844D	WT	*P value*
Liver	1.07 ± 0.57	1.03 ± 0.35	*0.94*	0.57 ± 0.29	0.60 ± 0.17	*0.87*	**0.40 ± 0.08**	**0.23 ± 0.06**	***0.03***
Brain	6.2 ± 0.9	7.7 ± 1.0	*0.170*	8.0 ± 4.8	7.8 ± 0.4	*0.881*	6.8 ± 0.7	7.4 ± 0.6	*0.298*
Spleen	6.1 ± 0.4	7.0 ± 1.0	*0.245*	7.3 (n = 1)	6.7 (n = 1)		5.3 ± 2.8	4.8 ± 3.2	*0.837*
Heart	7.4 ± 3.6	10.3 ± 1.3	*0.251*	6.7 ± 7.2	12.8 ± 1.2	*0.591*	7.1 ± 3.1	8.4 ± 0.8	*0.530*
Kidney	6.1 ± 1.8	3.6 ± 1.5	*0.137*	2.1 ± 1.5	5.0 ± 1.6	*0.085*	2.4 ± 2.0	1.9 ± 1.3	*0.723*
C18 DMA/C18:0									
	Day 15			3 months			6 months		
	Pex1-G844D	WT	*P value*	Pex1-G844D	WT	*P value*	Pex1-G844D	WT	*P value*
Liver	0.53 ± 0.25	0.47 ± 0.06	*0.68*	0.70 ± 0.26	0.83 ± 0.15	*0.49*	0.53 ± 0.13	0.40 ± 0.10	*0.22*
Brain	8.4 ± 1.4	9.5 ± 2.4	*0.519*	19.2 ± 11.3	15.7 ± 2.7	*0.283*	15.3 ± 2.1	16.6 ± 4.4	*0.619*
Spleen	4.4 ± 0.4	5.4 ± 1.1	*0.229*	5.9 (n = 1)	5.8 (n = 1)		5.2 ± 2.6	4.5 ± 1.7	*0.585*
Heart	1.3 ± 0.3	1.4 ± 0.1	*0.442*	2.7 ± 1.5	5.7 ± 0.3	*0.357*	**3.4 ± 0.3**	**4.6 ± 0.3**	***0.002***
Kidney	5.3 ± 0.4	6.5 ± 1.5	*0.245*	**3.4 ± 1.80**	**6.5 ± 0.4**	***0.044***	3.7 ± 1.4	5.6 ± 3.2	*0.133*

Shown are mean + SD determined in 3 animals per age group, except for some data of spleen of 3 months old mice ($n = 1$). Significant changes with P values < 0.05 are displayed in bold.
Concentrations of DHA are provided as nmol/mg protein, C26:0 as μmol/g protein, pristanic acid as μmol/g protein, phytanic acid as μmol/g protein, plasmalogens as ratio of C16– and C18 dimethyl acetal (DMA) over corresponding fatty acids, bile acids in pmol/mg protein in organs and μmol/l in plasma, and C26:0-lysoPC in nmol/l. C24-bile acids are the sum of cholic acid, chenodeoxycholic acid, deoxycholic acid, muricholic acid and ursodeoxycholic acid. C27-bile acids are the sum of dihydroxycholestanoic acid, trihydroxycholestanoic acid and tetrahydroxycholestanoic acid. n/a = not assessed.

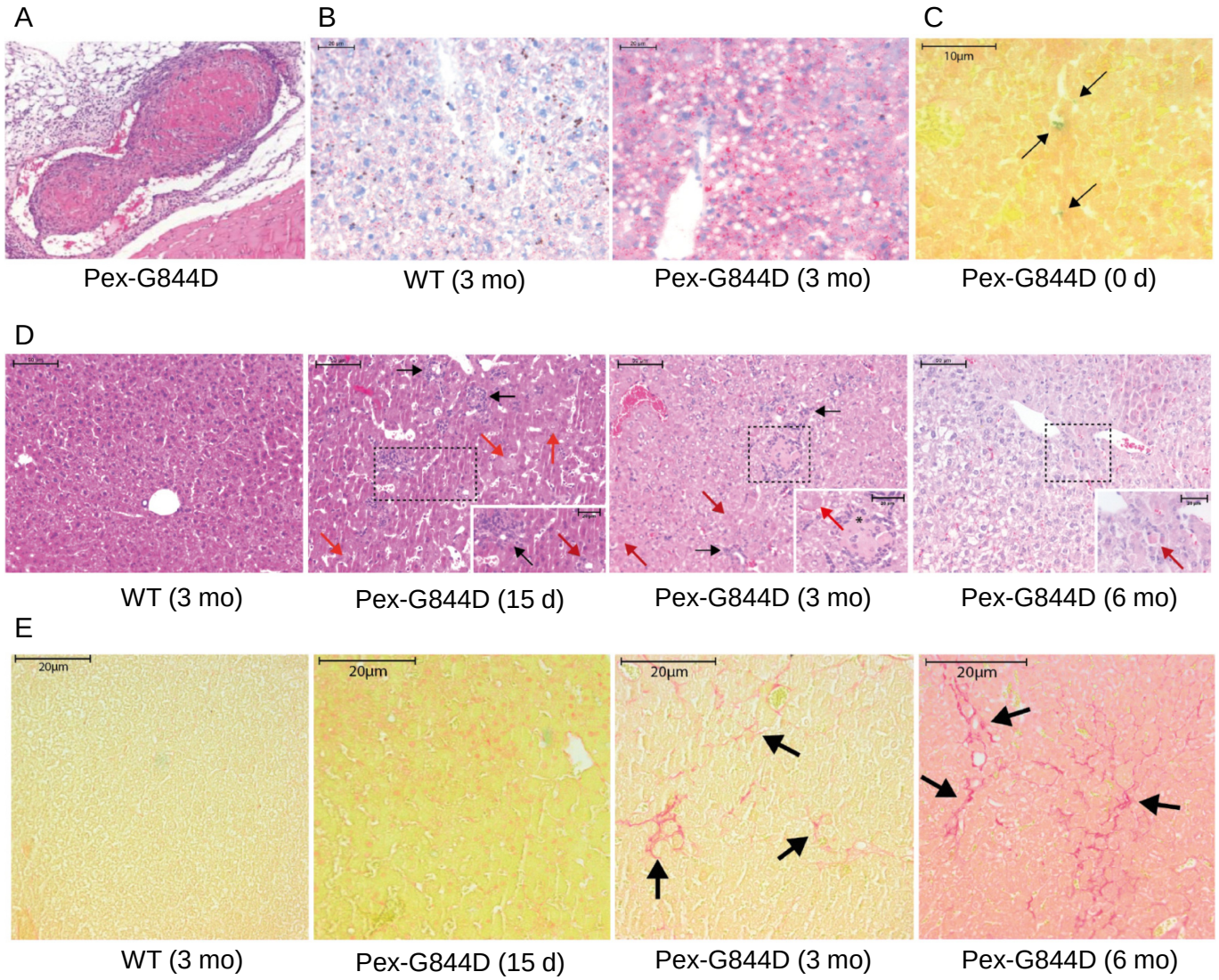

Fig. 3. Representative light-microscopy images of liver sections of wild type and Pex1-G844D mice. (A) Venous vascular wall inflammation and intravascular coagulation with complete occlusion of the vein in a cross section of spine from a 3 months old Pex1-G844D mice. Image is representative for other intravascular coagulation at different sites of the body, such as hepatic veins. (B) Liver tissue of 3-months old Pex1-G844D mice showed a more pronounced Oil Red O staining than liver tissue of wild type mice (bars 20 µm). (C) Positive Fouchet staining in livers of Pex1-G844D mice at birth showed clear accumulation of bile pigment (black arrows). (D) H&E staining of 3-months old wild type liver tissues showed normal hepatic architecture with components of basic liver lobules, with portal area and central venule. In 15-days old Pex1-G844D mice a change in liver morphology in noted with a lack of portal triads, inflammatory processes (black arrows), single cell necrosis (red arrow) and bile duct proliferation. In 3-months old Pex1-G844D liver tissues inflammatory processes (black arrows), single cell necrosis (dashed arrows) with early stage of liver cell dysplasia (upper part) and large necrotic processes (star) are observed. In 6-months old Pex1-G844D liver tissues a transition of normal hepatocytes to a focus of cellular alternation with increased nucleus-cytoplasma ratio is observed (bars 50 µm). (E) Development of hepatic fibrosis in 3 and 6 months old Pex1-G844D mice as illustrated by positive Sirius Red staining (black arrows).

bile acids in wild type liver are predominantly in the tauro-conjugated form. The unconjugated C_{27}-bile acid intermediates were also significantly increased in plasma, spleen, heart and kidney but not detectable in brain samples of Pex1-G844D mice at age 3 and 6 months.

Although the synthesis of plasmalogens involves the activity of two peroxisomal enzymes, their levels were overall not lowered in any of the tissues of the Pex1-G844D mice with the exception of liver samples of new-born mice at day 0 (Table 2D).

Given that in other peroxisome-deficient mouse models, deregulation of carbohydrate metabolism was found, we also tested blood glucose concentration in the Pex1-G844D mice. Interestingly, we found that plasma glucose levels in Pex1-G844D mice were markedly decreased at day 0 (mean: 0.7 mmol/l versus 3.6 mmol/l in heterozygous Pex1-G844D littermates; $p = 0.0015$; $n = 3$) and day 5 (mean: 2.5 mmol/l versus 6.0 mmol/l in wild type littermates; $p = 0.0002$; n = 3), demonstrating a hypoglycaemic state. Glycogen could be demonstrated in livers of Pex1-G844D mice at day 10, 15 and 3 months, but the intensity of staining was always less than in wild type mice of the same age (supplemental Fig. 1B).

3.4. Macroscopic and microscopic analyses of Pex1-G844D mice

For histological analysis we used tissues from mice aged 0, 5, 10 and 15 days, 3 and 6 months. After sacrificing the mice, all organs were examined macroscopically, and microscopically after hematoxylin and eosin (H&E) staining.

Macroscopic examinations revealed pronounced hepatomegaly in Pex1-G844D mice at 3 and 6 months of age (Supplemental Fig. 1C & D). In addition, nearly all Pex1-G844D mice showed unilateral hydronephrosis at all ages (not shown).

No major defects in the skin, skeleton, brain, heart, lung, spleen, stomach, intestine, pancreas and testis were found upon gross macroscopic examination. However, microscopic analysis revealed the presence of venous vascular wall inflammation, intravascular coagulation, the formation of thrombi with complete occlusion of the veins at different sites of the body in the Pex1-G844D mice at different ages (Fig. 3A). In liver tissues of the Pex1-G844D mice, we observed accumulation of small vesicles at 3- and 6 months, which by Oil Red O staining were shown to be composed of triglycerides/cholesterol esters (Fig. 3B). Positive Fouchet staining revealed the accumulation of bile pigment in livers of Pex1-G844D mice at day 0 (Fig. 3C), but this was not found at later ages. H&E stained sections of livers from 15 days old Pex1-G844D mice revealed single cell necrosis, bile duct proliferation and numerous inflammatory cells (Fig. 3D). The livers of 3 months old Pex1-G844D mice showed early stages of cellular dysplasia while the 6 months old mice showed a transition of normal hepatocytes to a focus of cellular alternation with increased nucleus-cytoplasm ratio (i.e. hepatic adenoma) (Fig. 3D). Sirius Red staining, used to determine liver fibrosis, was positive in the livers of 3 months old Pex1-G844D mice and even more pronounced at 6 months of age (Fig. 3E).

Because most biochemical and histological abnormalities were found in the livers of the Pex1-G844D mice, we performed electron microscopy analysis of livers of 5 days old Pex1-G844D mice. As shown in Fig. 4A, no morphologically recognizable peroxisomes were observed in the Pex1-G844D livers, although they contained tiny vesicles (black arrows), which may represent microperoxisomes. To determine if these vesicles could represent functional microperoxisomes capable of importing matrix proteins, we performed immunogold labelling with antibodies against peroxisomal thiolase. No gold particles were found associated with these vesicles, in contrast to peroxisomes in livers of wild type mice (Fig. 4B). This corresponds with the above described defect in thiolase processing in Pex1-G844D liver samples (Fig. 2C). Labelling of peroxisomes with antibodies against peroxisomal membrane proteins was not successful (data not shown). In addition to a deficiency of peroxisomes, we observed aberrant mitochondria, including swollen mitochondria with abnormal cristae in the Pex1-G844D liver samples. It has been reported that livers of ZSD patients also contain mitochondria with altered morphology and function [36,37].

3.5. Activity of mitochondrial complexes

Abnormal mitochondrial morphology and function has also been described in previously reported *Pex* mouse models with more severe phenotypes [31–33]. When we measured the activities of the

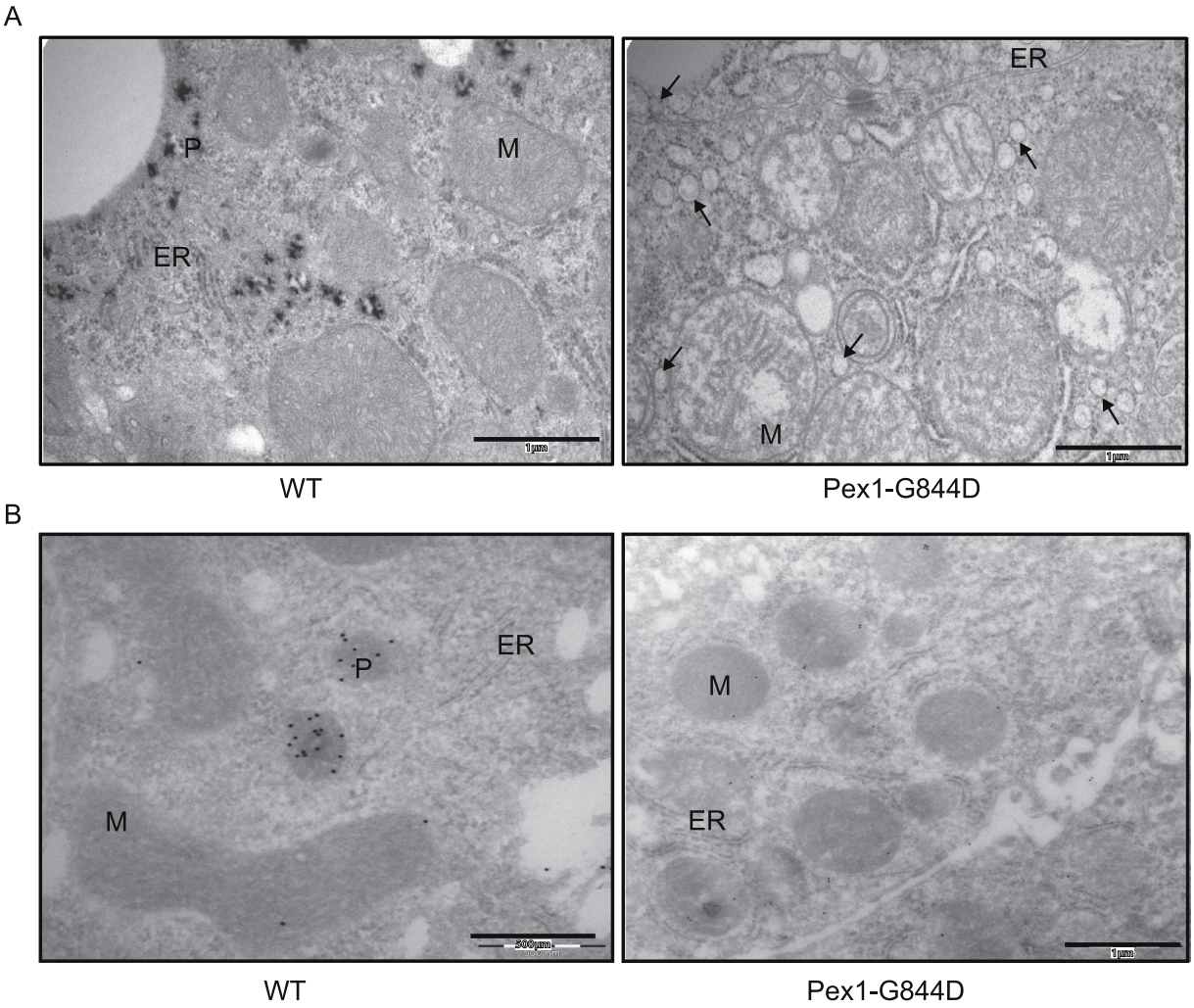

Fig. 4. Electron micrographs of liver sections of 5 days old wild type and Pex1-G844D mice. (A) Tissue embedded in Epon 812. Note the absence of identifiable peroxisomes (P), the presence of multiple tiny vesicles (black arrows) and abnormal mitochondria (M) in the Pex1-G844D liver in contrast to wild type. (B) Immunogold labelling with peroxisomal thiolase. Multiple gold particles are located in peroxisomes of wild type liver but absent in liver of the Pex1-G844D mice. ER, endoplasmic reticulum (For interpretation of the references to colour in this figure legend, the reader is referred to the web version of this article.)

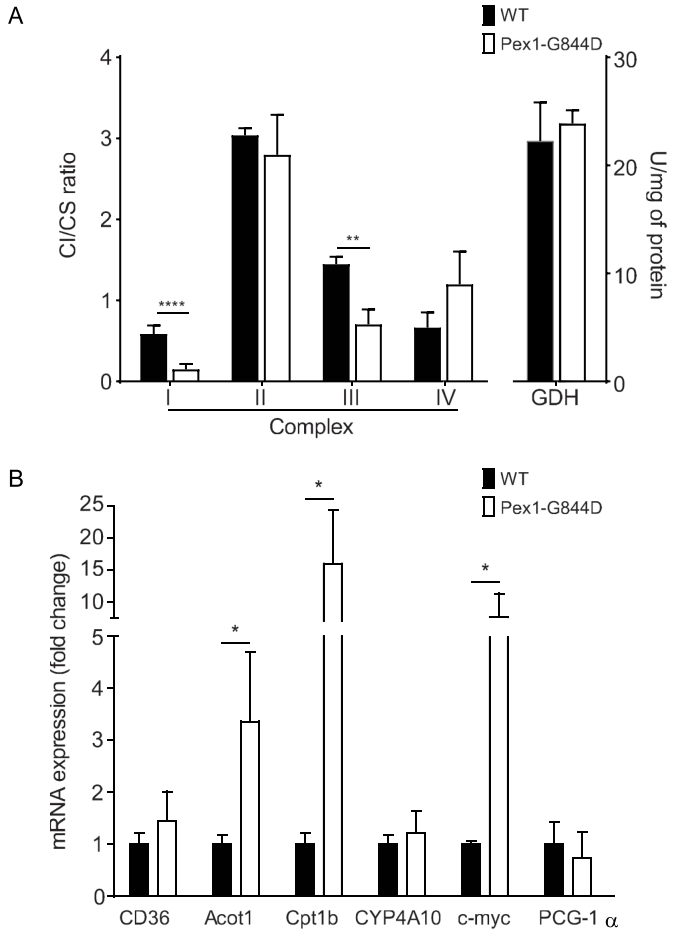

Fig. 5. Mitochondrial function in liver homogenates of 6 months old mice. (A) Activity measurements of the respiratory chain complexes (expressed as relative to the activity of citrate synthase (CS); left axis) showed significant decreased activities of complex I and III. Glutamate dehydrogenase (GDH) activities were similar (right axis). (B) qRT-PCR analysis of regulators of mitochondrial biogenesis and PPARα target genes revealed significantly increased expression of *Acot1*, *Cpt1b* and *c-myc*. All values are shown as mean ± SD. $^{*}P < 0.05$, $^{**}P < 0.01$, $^{****}P < 0.0001$.

mitochondrial matrix enzymes citrate synthase and glutamate dehydrogenase (Fig. 5A) in livers of Pex1-G844D mice, they were similar as in wild type mice. However, as previously reported for *Pex5* knockout livers [33] we observed a significant decrease in the activities of respiratory chain complex I and complex III whereas the activities of complex II and IV remained unchanged (Fig. 5A). These data corroborate the previous notion that peroxisomal dysfunction perturbs the structure and function of the inner mitochondrial membrane [31].

3.6. Transcriptional changes

It has been shown previously that a decreased or deficient peroxisomal β-oxidation can give rise to the accumulation of ligands that activate PPARα [38,39]. We also observed increased expression of several established PPARα target genes in livers of the Pex1-G844D mice including *Acot1, Cpt1b* and *c-myc* (a regulator of mitochondrial biogenesis and proto-oncogene). However, the expression of other established PPARα target genes such as *Cyp4a10* and *Cd36* was unaltered (Fig. 5B). We also did not observe changes in expression of *Pgc-1α*, the master regulator of mitochondrial biogenesis, in Pex1-G844D livers. A reduced expression of *Pgc-1α* was previously found in hepatocyte-specific *Pex5* knockout mice, which showed aberrant mitochondrial morphology and proliferation [33].

4. Discussion

We generated and characterized a hypomorphic mouse model for ZSDs, containing a homozygous Pex1-p.G844D allele, which is the equivalent of the most commonly found mutant allele in the human *PEX1* gene [6,7,15]. ZSD patients homozygous for this PEX1-p.G843D allele present with a relatively mild phenotype, characterized mainly by liver disease, developmental delay, and visual and hearing impairment, and may reach adulthood [2,3,20]. Our studies revealed that the homozygous Pex1-G844D mutation in mice also allows survival into adulthood, provided that the mice survive a critical phase during the lactation period, i.e. the first 20 postnatal days. This is in contrast to several previously reported *Pex* knock-out mice, generated by deleting different *Pex* genes, including *Pex2* [40], *Pex5* [41], *Pex10* [42] and *Pex13* [43], which represented the severe end of the ZSD spectrum and showed severe early-lethal phenotypes.

At birth, the Pex1-G844D mice and their wild-type/heterozygous littermates were indistinguishable in size and weight, suggesting normal embryonic development. However, analysis of the genotypes in the offspring of heterozygote breeding pairs demonstrates embryonal/perinatal loss of Pex1-G844D mice. We cannot exclude that weak pups had been eaten by the mother before litters were visually examined, as this is not uncommon for C57BL/6 strains [44]. As far as we know, embryonic loss of foetuses affected with ZSD has not been noted in humans.

After birth, the Pex1-G844D mice showed a clear growth delay, which becomes apparent from P3. We noted that in particular the first 20 days of life are critical for the survival of Pex1-G844D mice, as 75% of the mice died before P20. Several causes may contribute to this high mortality rate. First, we noted that few hours after birth, the Pex1-G844D pups had very low plasma glucose levels, indicating a severe hypoglycemic state. This could be related to the mitochondrial dysfunction we observed in the livers of the Pex1-G844D mice, which may result in a higher demand of glucose for energy production, as hypothesized previously [39]. Second, the observed weakness may cause difficulty in feeding, causing reduced food intake and a caloric deficit. Third, the decreased levels of C_{24} bile acids in conjunction with the increase in C_{27} bile acid intermediates and the occurrence of liver cholestasis in Pex1-G844D pups may cause problems in digestion of the fat that is present in the mother milk, causing further malabsorption [45]. In this respect it is important to note that after P20, when the Pex1-G844D mice switch to normal chow containing primarily carbohydrates and hardly fat, survival was nearly 100%. Finally, in some mice we observed venous thrombi, especially in the liver, with complete occlusion of veins and intravascular wall inflammation, which may also be a cause of early death. The formation of these venous thrombi could be a consequence of liver failure and subsequent disseminated intravascular coagulation [46,47].

Our combined findings showed that in particular the liver is affected in the Pex1-G844D mouse, whereas other tissues are relatively spared. Biochemically, this follows from the complete defect in thiolase processing in liver samples indicating the absence of matrix-protein import competent peroxisomes, which was also confirmed by electron microscopy of livers of 5 days old Pex1-G844D mice. In most other tissues, thiolase processing was normal implying that, in contrast to liver, these tissues still contain functional peroxisomes. Selective peroxisome deficiency in liver also has been observed in patients with a milder ZSD presentation and homozygous for the G843D mutation in *PEX1* [48 and unpublished data]. At the metabolite level, we also observed consistent elevations of C26:0 and C_{27}-bile acid intermediates only in the liver samples of Pex1-G844D mice at all ages, while the levels of these and other metabolites fluctuate and often are normal in other tissues. We found the levels of C26:0, DHA and plasmalogens also to be normal in brain at most ages. This contrasts with findings in generalized *Pex* knockout mice in which reduced levels of plasmalogens were found in liver as well as brain [40,41,43]. The reason for the selective ablation of

functional hepatic peroxisomes is unclear, but may be due to the liver-specific accumulation of toxic bile acid intermediates and/or cholestasis, which may affect the conformation/functioning of the Pex1-G844D protein causing a complete block in peroxisomal matrix protein import. Previous work has shown that the function of human PEX1-G843D protein is sensitive to unfavorable conditions, including elevated temperature, but can be stabilized by lower temperatures or small molecules, which leads to improved peroxisomal matrix protein import in PEX1-G843D cells [17–19].

The most prominent histological abnormalities observed in almost all Pex1-G844D mice analyzed at the different ages were hydronephrosis and liver abnormalities, including cholestasis. At later ages, the mice presented with hepatomegaly, bile duct proliferation with inflammation leading to liver fibrosis and even the formation of hepatic adenomas in adulthood. The hepatomegaly may be the result of the upregulation of the PPARα target gene *c-myc*, as previously suggested for other mice [33]. Unexpectedly, however, we found that only a subset of PPARα target genes, i.e. *Cpt1b*, *Acot1* and *c-myc*, were induced in livers of 6 months old Pex1-G844D mice whereas others, i.e. *Cd36* and *Cyp4a10* were normally expressed.

In addition to the absence of functional peroxisomes in the liver, we also observed an altered morphology of hepatic mitochondria, including a swollen appearance and loss of cristae, which biochemically was associated with altered activities of some mitochondrial complexes. Although the underlying cause of this mitochondrial dysfunction is unknown [33], it should be noted that similar mitochondrial alterations have also been reported in patients with Zellweger syndrome [36,37].

While our analysis was in progress, the generation and initial characterization of a similar mouse model also harbouring the homozygous *Pex1*-c.2531G > A (p.G844D) mutation was reported, prompting us to a more thorough analysis of our mouse model [49]. Characterization of the other mouse model revealed several similarities with our mouse model including growth retardation, elevated C26:0-lysoPC in bloodspots, C_{27}-bile acid intermediates in liver and plasma, and bile duct proliferation on H&E liver histology. Overall, however, the other model showed a much milder phenotype with a survival rate of 100% until P12. After P12, however, 20 out of 49 mice died with a median survival of 22 days also suggesting a critical survival period around P20. The difference in survival rate and phenotype most probably relates to the fact that our model is on a pure C57BL/6N genetic background, whereas the previously reported model has a mixed 129 × C57BL/6 × C57BL/6N genetic background. Importantly, however, our more detailed analyses showed that liver disease due to defective hepatic peroxisomes is the predominant outcome in the Pex1-G844D mouse, while peroxisomal functions in many other tissues appeared hardly affected.

Comparison of our findings in the mouse to those in human *PEX1* patients, who are homozygous for the *PEX1*-c.2528G > A (p.G843D) mutation, reveals important similarities. First, the mice showed overall weakness at birth and a critical survival phase followed by growth retardation, if they survived this phase. This weakness may represent hypotonia causing failure to thrive, which is also an important clinical symptom in new-born ZSD babies. Second, we recently reported that peroxisomal metabolites in plasma may show marked fluctuations in mild human ZSD patients during life with some adult patients even displaying an almost completely normalized biochemical profile [20]. In the mice, we also observed metabolite fluctuations at the organ level. Third, skin fibroblasts of mild ZSD patients typically show peroxisomal mosaicism, which we also observe in the MEFs of our mouse model. Finally, liver disease is an important aspect of the human disease and liver cirrhosis has been described in multiple ZSD patients [2,3,14,50].

In summary, the hypomorphic Pex1-G844D mouse model shows many disease-specific aspects also observed in mild ZSD patients with liver disease as predominant symptom. This model thus can be used to study the pathogenesis, especially the liver phenotype in more detail and to test newly developed therapies, such as supplementation of small molecules that have been shown to improve peroxisomal functions in PEX1-G843D cells of ZSD patients [18,19]. It will be interesting to examine whether at later ages these mice also develop neurological abnormalities, such as polyneuropathy and leukoencephalopathy, that are observed in patients.

Supplementary data to this article can be found online at https://doi.org/10.1016/j.bbadis.2019.06.013.

Transparency document

The Transparency document associated with this article can be found, in online version.

Acknowledgements

We thank Merel Ebberink for helpful discussions and Petra Mooijer and Wicky Tigchelaar for valuable contributions to the paper. This work was supported by research grants from Hersenstichting Nederland (grant number F2012(1)-102) and E-Rare-3 PERescue (ZonMW # 9003037605) to H.R.W., Stichting Steun Emma Kinderziekenhuis AMC (grant nr WAR012-2015-03-003) to B.T.P-T and Stichting Metakids (grant nr 2014-049) to B.T.P-T and H.R.W.

References

[1] R.J. Wanders, H.R. Waterham, Biochemistry of mammalian peroxisomes revisited, Annu. Rev. Biochem. 75 (2006) 295–332.
[2] F.C. Klouwer, K. Berendse, S. Ferdinandusse, R.J. Wanders, M. Engelen, B.T. Poll-The, Zellweger spectrum disorders: clinical overview and management approach, Orphanet J Rare Dis. 10 (2015) 151.
[3] N.E. Braverman, G.V. Raymond, W.B. Rizzo, A.B. Moser, M.E. Wilkinson, E.M. Stone, S.J. Steinberg, M.F. Wangler, E.T. Rush, J.G. Hacia, M. Bose, Peroxisome biogenesis disorders in the Zellweger spectrum: an overview of current diagnosis, clinical manifestations, and treatment guidelines, Mol. Genet. Metab. 117 (2016) 313–321.
[4] A. Raas-Rothschild, R.J. Wanders, P.A. Mooijer, J. Gootjes, H.R. Waterham, A. Gutman, Y. Suzuki, N. Shimozawa, N. Kondo, G. Eshel, M. Espeel, F. Roels, S.H. Korman, A PEX6-defective peroxisomal biogenesis disorder with severe phenotype in an infant, versus mild phenotype resembling Usher syndrome in the affected parents, Am. J. Hum. Genet. 70 (2002) 1062–1068.
[5] I. Ratbi, K.D. Falkenberg, M. Sommen, N. Al-Sheqaih, S. Guaoua, G. Vandeweyer, J.E. Urquhart, K.E. Chandler, S.G. Williams, N.A. Roberts, M. El Alloussi, G.C. Black, S. Ferdinandusse, H. Ramdi, A. Heimler, A. Fryer, S.A. Lynch, N. Cooper, K.R. Ong, C.E. Smith, C.F. Inglehearn, A.J. Mighell, C. Elcock, J.A. Poulter, M. Tischkowitz, S.J. Davies, A. Sefiani, A.A. Mironov, W.G. Newman, H.R. Waterham, G. Van Camp, Heimler syndrome is caused by hypomorphic mutations in the peroxisome-biogenesis genes PEX1 and PEX6, Am. J. Hum. Genet. 97 (2015) 535–545.
[6] H.R. Waterham, M.S. Ebberink, Genetics and molecular basis of human peroxisome biogenesis disorders, Biochim. Biophys. Acta 1822 (9) (2012 Sep) 1430–1441.
[7] S.J. Steinberg, G.V. Raymond, N.E. Braverman, A.B. Moser, Zellweger spectrum disorder. 2003 Dec 12 [updated 2017 Dec 21], in: M.P. Adam, H.H. Ardinger, R.A. Pagon, S.E. Wallace, Bean LJH, K. Stephens, A. Amemiya (Eds.), GeneReviews® [Internet], University of Washington, Seattle, Seattle (WA), 1993–2018.
[8] R.J. Wanders, F.C. Klouwer, S. Ferdinandusse, H.R. Waterham, Poll-Thé BT. Clinical and laboratory diagnosis of peroxisomal disorders, Methods Mol. Biol. 1595 (2017) 329–342.
[9] F. Roels, M. Espeel, D. De Craemer, Liver pathology and immunocytochemistry in congenital peroxisomal diseases: a review, J. Inherit. Metab. Dis. 14 (1991) 853–875.
[10] F. Roels, M. Espeel, F. Poggi, H. Mandel, L. van Maldergem, J.M. Saudubray, Human liver pathology in peroxisomal diseases: a review including novel data, Biochimie. 75 (1993) 281–292.
[11] M. Baes, P.P. Van Veldhoven, Hepatic dysfunction in peroxisomal disorders, Biochim. Biophys. Acta 1863 (2016) 956–970.
[12] M.H. Keane, H. Overmars, T.M. Wikander, S. Ferdinandusse, M. Duran, R.J. Wanders, P.L. Faust, Bile acid treatment alters hepatic disease and bile acid transport in peroxisome-deficient PEX2 Zellweger mice, Hepatology 45 (2007) 982–997.
[13] S. Ferdinandusse, S. Denis, P.L. Faust, R.J. Wanders, Bile acids: the role of peroxisomes, J. Lipid Res. 50 (2009) 2139–2147.
[14] S. Ferdinandusse, S. Denis, G. Dacremont, R.J. Wanders, Toxicity of peroxisomal C27-bile acid intermediates, Mol. Genet. Metab. 96 (2009) 121–128.
[15] M.S. Ebberink, P.A. Mooijer, J. Gootjes, J. Koster, R.J. Wanders, H.R. Waterham, Genetic classification and mutational spectrum of more than 600 patients with a Zellweger syndrome spectrum disorder, Hum. Mutat. 32 (2011) 59–69.
[16] N. Miyata, Y. Fujiki, Shuttling mechanism of peroxisome targeting signal type 1 receptor Pex5: ATP-independent import and ATP-dependent export, Mol. Cell. Biol. 25 (2005) 10822–11032.

[17] A. Imamura, S. Tamura, N. Shimozawa, Y. Suzuki, Z. Zhang, T. Tsukamoto, T. Orii, N. Kondo, T. Osumi, Y. Fujiki, Temperature-sensitive mutation in PEX1 moderates the phenotypes of peroxisome deficiency disorders, Hum. Mol. Genet. 7 (1998) 2089–2094.
[18] R. Zhang, L. Chen, S. Jiralerspong, A. Snowden, S. Steinberg, N. Braverman, Recovery of PEX1-Gly843Asp peroxisome dysfunction by small-molecule compounds, Proc. Natl. Acad. Sci. U. S. A. 107 (2010) 5569–5574.
[19] K. Berendse, M.S. Ebberink, L. Ijlst, B.T. Poll-The, R.J. Wanders, H.R. Waterham, Arginine improves peroxisome functioning in cells from patients with a mild peroxisome biogenesis disorder, Orphanet J Rare Dis. 8 (2013) 138.
[20] K. Berendse, M. Engelen, S. Ferdinandusse, C.B. Majoie, H.R. Waterham, F.M. Vaz, J.H. Koelman, P.G. Barth, R.J. Wanders, B.T. Poll-The, Zellweger spectrum disorders: clinical manifestations in patients surviving into adulthood, J. Inherit. Metab. Dis. 39 (2016) 93–106.
[21] G.J. Todaro, Quantitative studies of the growth of mouse embryo cells in culture and their development into established lines, J. Cell Biol. 17 (1963) 299–313.
[22] M.J. Tymms, I. Kola, Isolation of embryonic fibroblasts and their use in the in vitro characterization of gene function, Gene Knockout Protocols, vol. 158, 2001, pp. 205–215.
[23] E.G. van Grunsven, E. van Berkel, P.A. Mooijer, P.A. Watkins, H.W. Moser, Y. Suzuki, L.L. Jiang, T. Hashimoto, G. Hoefler, J. Adamski, R.J. Wanders, Peroxisomal bifunctional protein deficiency revisited: resolution of its true enzymatic and molecular basis, Am. J. Hum. Genet. 64 (1999) 99–107.
[24] R.J. Wanders, S. Denis, J.P. Ruiter, R.B. Schutgens, C.W. van Roermund, B.S. Jacobs, Measurement of peroxisomal fatty acid beta-oxidation in cultured human skin fibroblasts, J. Inherit. Metab. Dis. 18 (Suppl. 1) (1995) 113–124.
[25] R. Ofman, R.J. Wanders, Purification of peroxisomal acyl-CoA: dihydroxyacetonephosphate acyltransferase from human placenta, Biochim. Biophys. Acta 1206 (1994) 27–34.
[26] N. van der Wel, D. Hava, D. Houben, D. Fluitsma, M. van Zon, J. Pierson, M. Brenner, P.J. Peters, M. tuberculosis and M. leprae translocate from the phagolysosome to the cytosol in myeloid cells, Cell. 129 (2007) 1287–1298.
[27] P. Vreken, A.E. van Lint, A.H. Bootsma, H. Overmars, R.J. Wanders, A.H. van Gennip, Rapid stable isotope dilution analysis of very-long-chain fatty acids, pristanic acid and phytanic acid using gas chromatography-electron impact mass spectrometry, J Chromatogr B Biomed Sci Appl. 713 (1998) 281–287.
[28] A.H. Bootsma, H. Overmars, A. van Rooij, A.E. van Lint, R.J. Wanders, A.H. van Gennip, P. Vreken, Rapid analysis of conjugated bile acids in plasma using electrospray tandem mass spectrometry: application for selective screening of peroxisomal disorders, J. Inherit. Metab. Dis. 22 (1999) 307–310.
[29] G. Dacremont, G. Vincent, Assay of plasmalogens and polyunsaturated fatty acids (PUFA) in erythrocytes and fibroblasts, J. Inherit. Metab. Dis. 18 (Suppl. 1) (1995) 84–89.
[30] Hubbard WC, Moser AB, Liu AC, Jones RO, Steinberg SJ, Lorey F, Panny SR, Vogt RF Jr, Macaya D, Turgeon CT, Tortorelli S, Raymond GV. Newborn screening for X-linked adrenoleukodystrophy (X-ALD): validation of a combined liquid chromatography-tandem mass spectrometric (LC-MS/MS) method. Mol. Genet. Metab. 2009; 97:212–220.
[31] R. Dirkx, I. Vanhorebeek, K. Martens, A. Schad, M. Grabenbauer, D. Fahimi, P. Declercq, P.P. Van Veldhoven, M. Baes, Absence of peroxisomes in mouse hepatocytes causes mitochondrial and ER abnormalities, Hepatology. 41 (2005) 868–878.
[32] E. Baumgart, I. Vanhorebeek, M. Grabenbauer, M. Borgers, P.E. Declercq, H.D. Fahimi, M. Baes, Mitochondrial alterations caused by defective peroxisomal biogenesis in a mouse model for Zellweger syndrome (PEX5 knockout mouse), Am. J. Pathol. 159 (2001) 1477–1494.
[33] A. Peeters, A.B. Shinde, R. Dirkx, J. Smet, K. De Bock, M. Espeel, I. Vanhorebeek, A. Vanlander, R. Van Coster, P. Carmeliet, M. Fransen, P.P. Van Veldhoven, M. Baes, Mitochondria in peroxisome-deficient hepatocytes exhibit impaired respiration, depleted DNA, and PGC-1α independent proliferation, Biochim. Biophys. Acta 1853 (2015) 285–298.
[34] I.V. Kurochkin, Y. Mizuno, A. Konagaya, Y. Sakaki, C. Schönbach, Y. Okazaki, Novel peroxisomal protease Tysnd1 processes PTS1- and PTS2-containing enzymes involved in beta-oxidation of fatty acids, EMBO J. 26 (2007) 835–845.
[35] F.C.C. Klouwer, S. Ferdinandusse, H. van Lenthe, W. Kulik, R.J.A. Wanders, B.T. Poll-The, H.R. Waterham, F.M. Vaz, Evaluation of C26:0-lysophosphatidylcholine and C26:0-carnitine as diagnostic markers for Zellweger spectrum disorders, J. Inherit. Metab. Dis. 40 (2017) 875–881.
[36] S. Goldfischer, C.L. Moore, A.B. Johnson, A.J. Spiro, M.P. Valsamis, H.K. Wisniewski, R.H. Ritch, W.T. Norton, I. Rapin, L.M. Gartner, Peroxisomal and mitochondrial defects in the cerebro-hepato-renal syndrome, Science. 182 (1973) 62–64.
[37] V. Salpietro, R. Phadke, A. Saggar, I.P. Hargreaves, R. Yates, C. Fokoloros, K. Mankad, J. Hertecant, M. Ruggieri, D. McCormick, M. Kinali, Zellweger syndrome and secondary mitochondrial myopathy, Eur. J. Pediatr. 174 (2015) 557–563.
[38] C.Y. Fan, J. Pan, N. Usuda, A.V. Yeldandi, M.S. Rao, J.K. Reddy, Steatohepatitis, spontaneous peroxisome proliferation and liver tumors in mice lacking peroxisomal fatty acyl-CoA oxidase. Implications for peroxisome proliferator-activated receptor alpha natural ligand metabolism, J. Biol. Chem. 273 (1998) 15639–15645.
[39] A. Peeters, J.V. Swinnen, P.P. Van Veldhoven, M. Baes, Hepatosteatosis in peroxisome deficient liver despite increased β-oxidation capacity and impaired lipogenesis, Biochimie. 93 (2011) 1828–1838.
[40] P.L. Faust, M.E. Hatten, Targeted deletion of the PEX2 peroxisome assembly gene in mice provides a model for Zellweger syndrome, a human neuronal migration disorder, J. Cell Biol. 139 (1997) 1293–1305.
[41] M. Baes, P. Gressens, E. Baumgart, P. Carmeliet, M. Casteels, M. Fransen, P. Evrard, D. Fahimi, P.E. Declercq, D. Collen, P.P. van Veldhoven, G.P. Mannaerts, A mouse model for Zellweger syndrome, Nat. Genet. 17 (1997) 49–57.
[42] M.G. Hanson, V.L. Fregoso, J.D. Vrana, C.L. Tucker, L.A. Niswander, Peripheral nervous system defects in a mouse model for peroxisomal biogenesis disorders, Dev. Biol. 395 (2014) 84–95.
[43] M. Maxwell, J. Bjorkman, T. Nguyen, P. Sharp, J. Finnie, C. Paterson, I. Tonks, B.C. Paton, G.F. Kay, D.I. Crane, Pex13 inactivation in the mouse disrupts peroxisome biogenesis and leads to a Zellweger syndrome phenotype, Mol. Cell. Biol. 23 (2003) 5947–5957.
[44] E.M. Weber, B. Algers, H. Würbel, J. Hultgren, I.A.S. Olsson, Influence of strain and parity on the risk of litter loss in laboratory mice, Reprod. Domest. Anim. 48 (2013) 292–296.
[45] C.H. Knight, E. Maltz, A.H. Docherty, Milk yield and composition in mice: effects of litter size and lactation number, Comp. Biochem. Physiol. A Comp. Physiol. 84 (1986) 127–133.
[46] C.M. Bakker, E.A. Knot, J. Stibbe, J.H. Wilson, Disseminated intravascular coagulation in liver cirrhosis, J. Hepatol. 15 (1992) 330–335.
[47] M. Levi, Pathogenesis and diagnosis of disseminated intravascular coagulation, Int. J. Lab. Hematol. 40 (Suppl. 1) (2018) 15–20.
[48] M. Espeel, H. Mandel, F. Poggi, J.A. Smeitink, R.J. Wanders, I. Kerckaert, R.B. Schutgens, J.M. Saudubray, B.T. Poll-The, F. Roels, Peroxisome mosaicism in the livers of peroxisomal deficiency patients, Hepatology 22 (1995) 497–504.
[49] S. Hiebler, T. Masuda, J.G. Hacia, A.B. Moser, P.L. Faust, A. Liu, N. Chowdhury, N. Huang, A. Lauer, J. Bennett, P.A. Watkins, D.J. Zack, N.E. Braverman, G.V. Raymond, S.J. Steinberg, The PEX1-G844D mouse: a model for mild human Zellweger spectrum disorder, Mol. Genet. Metab. 111 (2014) 522–532.
[50] R.J. Wanders, S. Ferdinandusse, Peroxisomes, peroxisomal diseases, and the hepatotoxicity induced by peroxisomal metabolites, Curr. Drug Metab. 13 (2012) 1401–1411.